Ahmed S. Yousif
Mechanical Engineering Department, University of Technology, Baghdad, Iraq
20173@Uotechnology.edu.iq

Ammar S. Mohammed
Electrical Engineering Department, University of Technology, Baghdad, Iraq

Received on: 19/06/2017
Accepted on: 05/04/2018
Published online: 25/10/2018

Analysis and Simulation of Unmanned Aircraft Propeller Motor Using PSIM

Abstract- *The study and simulation of a PI speed controller for small UAV or quadcopter motor is discussed in this research. The motor under consideration is MAXON 2260 215, which is a brushless DC motor that has permanent magnets on the rotating part and the stationary windings are connected so that the back electromotive force is trapezoidal. The motor utilizes a PI controller, which dominate the duty cycle of the PWM pulses applied on the switches of the inverter so that the motor can run at the required speed. A Chopper is used as a power converter and a proportional–integral as speed and current controller. The DC motor, which is being run individually, can be controlled on a wide range of operation up to the rated speed. The simulation is implemented and evaluated using PSIM software program under a wide range of speed, voltage and load torque inputs such as the rated speed and load torque, half the rated load torque and half speed since these tests are vital to test maneuver movement such as roll, pitch, yaw and throttle. The main objectives of this paper are; to understand the process of deriving the model for a propeller motor, to evaluate the stability and accuracy of the control loop for successful aviation, to apply a tuning plan on a closed loop system (PI) and to check the system procedure versus the given technical specifications.*

Keywords- *PSIM, quadcopter, Propeller, PWM, PI, Motor, simulation*

How to cite this article: A.S. Yousif and A.S. Mohammed, "Analysis and Simulation of Aircraft Propeller Motor Using PSIM," *Engineering and Technology Journal*, Vol. 36, Part A, No. 10, pp. 1081-1090, 2018.

1. Introduction

An aircraft propeller is device that converts rotary motion from a motor to propulsive force. A typical propeller consists of a hub that rotates with the motor and two or more airfoil-section blades that are attached radially to the hub. The whole assembly rotates freely with the motor or engine shaft. Figure 1 shows a typical aircraft propeller. A DC motor is used to drive the propeller in the desired speed. A DC motor is a (One Input and One Output) system of torque and speed specifications that are matched with most mechanical applications [1]. As a result, a D.C motor can be managed over a wide range of speeds by adjusting the voltage of the terminal correctly [2]. Induction motors, Brushless DC motors and Synchronous motors are widely used in electric traction system. Thus, DC motors are always an outstanding solution for any sophisticated control project due to their well-established theory. To control the speed in any individually excited DC motor, the armature voltage is changed to values below the rated speed. This can be achieved by varying the values of the field flux in order to reach a speed that is higher than the rated speed [3]. The PI based speed control is preferred due to its quick control, affordable price and simple structure. In general, to control the speed of a DC motor the armature voltage must be varied below and up to the rated speed while fixing the field voltage value [4]. The output speed and the reference speed are compared and the error signal is fed to speed controller. The output of the controller can change any time there is a difference in the reference speed and the speed feedback. The speed controller's outcome is a voltage that controls the operation of the duty cycle, where the chopper is the converter. The converter output gives Va required to accelerate the motor return to the required speed. The reference speed is provided through a potential divider because the voltage from potential divider is related linearly to the speed of the DC motor. The output speed of motor is measured by Tacho-generator and since Tacho voltage will not be perfectly DC and will have some ripple. Therefore, it is required to add a filter with gain to bring Tacho output back to controller level [4-6.[

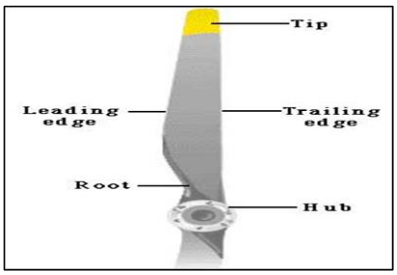

Figure 1: Aircraft Propeller

https://doi.org/10.30684/etj.36.10A.9
2412-0758/University of Technology-Iraq, Baghdad, Iraq

2. Analysis and Simulation

An electronic circuit simulation package (PSIM) is used to perform the simulation. It is specially made for the imitation of power electronics and the simulations of motor drives. However, it can be utilized to simulate any electronic circuit. PSIM utilizes nodal analysis and trapezoidal rule integration as a foundation for the simulation algorithm. Figure 2 shows the main program window.

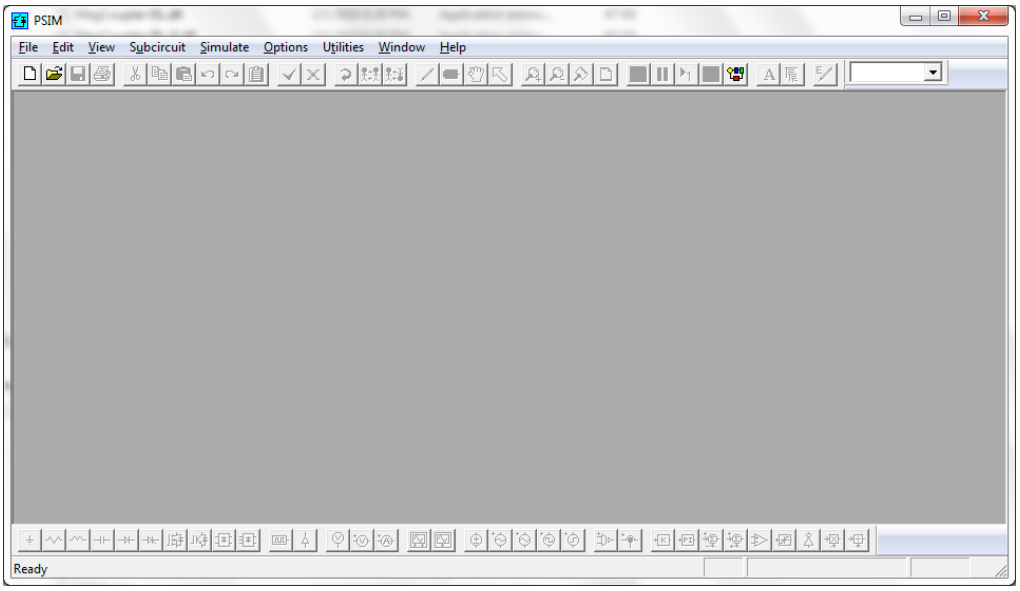

Figure 2: PSIM Main Window

PSIM also offers a schematic capture interface and a waveform viewer called Simview. PSIM has a lot of modules which increases its ability into detailed areas of circuit simulation and design such as control theory [7], electric motors [8], photovoltaics [9] and wind turbines [10]. PSIM is used by many companies in their projects and product development centers and it is used by universities for teaching and research.

I. Architecture of the DC Motor Control System

Figure 3 below shows the system under consideration. For this type of servo mechanical system, the current (and therefore the torque) should be controlled in order to avoid lurching and vibrations, which can be destructive for the motor. The classical two-loop structure will be used with one inner loop and one outer loop. The flowchart of the control loops is shown in Figure 4:

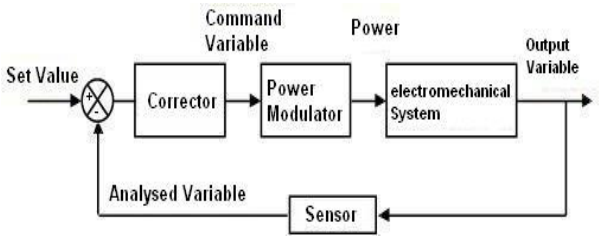

Figure 3: Architecture of the system

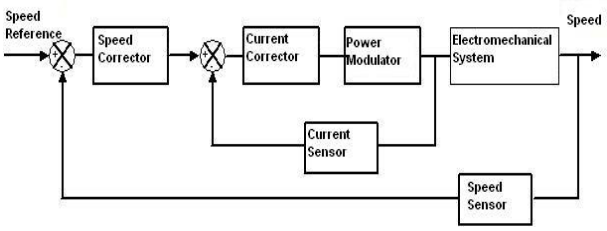

Figure 4: Flowchart of the Control Loop for the DC motor

After the system is modeled, the simulation tool can be used to analyze the behavior, adjust the controllers and carry out non-destructive tests on the motor, the following steps will be considered:

- Search for variables associated with the operating point.
- Modelling of the motor and the load.
- Modelling of the dc chopper.
- Identification of the response signal and adjustment of the controller.
- Identification of the response in terms of speed and adjustment of the controller.
- Setting limitations on voltage and current, defining the field of application.
- Analysis of the results and tests on the real structure.

II. Modelling of the Motor and Load

A separately excited dc machine with the constant flux will be used to model a dc permanent magnet

motor in PSIM. Figure 5 shows model dimensions, while Table 1 shows motor data. Figure 6 shows the rage of operation of this motor and Table 2 shows the specifications of the MAXON 2260 215 motor [11-13]:

F 2260 ∅60 mm, Graphite Brushes, 40 Watt

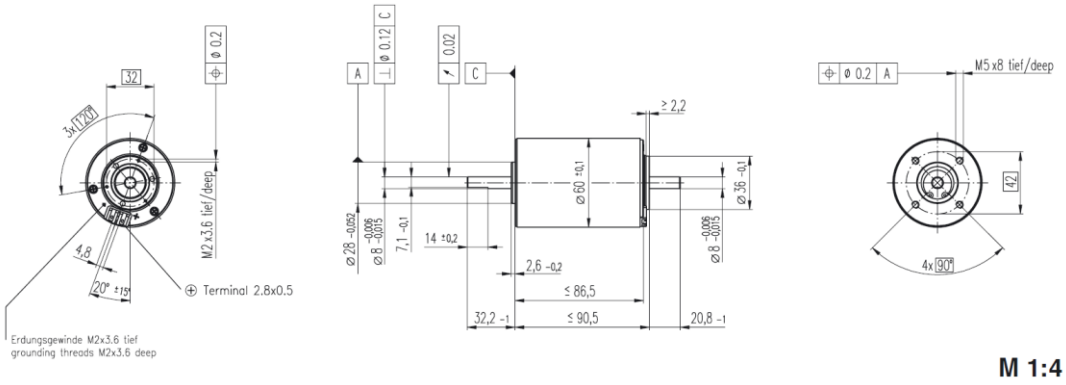

Figure 5: Maxon 2260 215 Dimensions

Table 1: Motor Data

Stock program
Standard program
Special program (on request!)

Order Number

2260. ... -51.216-200 (Insert winding number)

Winding number		811	812	813	814	815	816	817	818	810	819	820
Motor Data												
1 Assigned power rating	W	40	40	40	40	40	40	40	40	40	40	40
2 Nominal voltage	Volt	18.0	18.0	24.0	30.0	36.0	36.0	36.0	48.0	48.0	48.0	48.0
3 No load speed	rpm	4500	3450	3660	4270	4580	3630	2950	3190	2590	2090	1630
4 Stall torque	Nm	0.870	0.707	0.758	0.868	0.916	0.733	0.591	0.633	0.514	0.407	0.312
5 Speed / torque gradient	rpm / mNm	5.41	5.11	5.01	5.07	5.14	5.10	5.17	5.19	5.21	5.34	5.48
6 No load current	mA	387	283	225	215	194	147	117	95	75	60	46
7 Starting current	A	23.8	14.8	12.6	13.4	12.6	7.97	5.24	4.53	3.00	1.93	1.16
8 Terminal resistance	Ohm	0.755	1.21	1.91	2.25	2.87	4.52	6.87	10.6	16.0	24.9	41.2
9 Max. permissible speed	rpm	5000	5000	5000	5000	5000	5000	5000	5000	5000	5000	5000
10 Max. continuous current	A	3.30	2.67	2.16	1.99	1.77	1.43	1.17	0.945	0.771	0.621	0.484
11 Max. continuous torque	mNm	120	127	130	130	129	132	132	132	132	131	130
12 Max. power output at nominal voltage	W	98.2	61.2	70.4	94.4	107	67.8	44.4	51.6	33.9	21.5	12.8
13 Max. efficiency	%	73	72	73	75	75	74	71	73	70	67	64
14 Torque constant	mNm / A	36.5	47.6	60.3	65.0	73.0	92.0	113	140	171	211	268
15 Speed constant	rpm / V	262	201	158	147	131	104	84.8	68.4	55.7	45.3	35.6
16 Mechanical time constant	ms	36	36	35	35	34	34	34	34	34	34	34
17 Rotor inertia	gcm²	638	666	665	651	638	641	630	623	620	604	589
18 Terminal inductance	mH	0.23	0.39	0.63	0.73	0.92	1.46	2.18	3.36	5.05	7.66	12.40
19 Thermal resistance housing-ambient	K / W	5.0	5.0	5.0	5.0	5.0	5.0	5.0	5.0	5.0	5.0	5.0
20 Thermal resistance rotor-housing	K / W	2.4	2.4	2.4	2.4	2.4	2.4	2.4	2.4	2.4	2.4	2.4
21 Thermal time constant winding	s	73	76	76	74	73	73	72	71	71	69	67

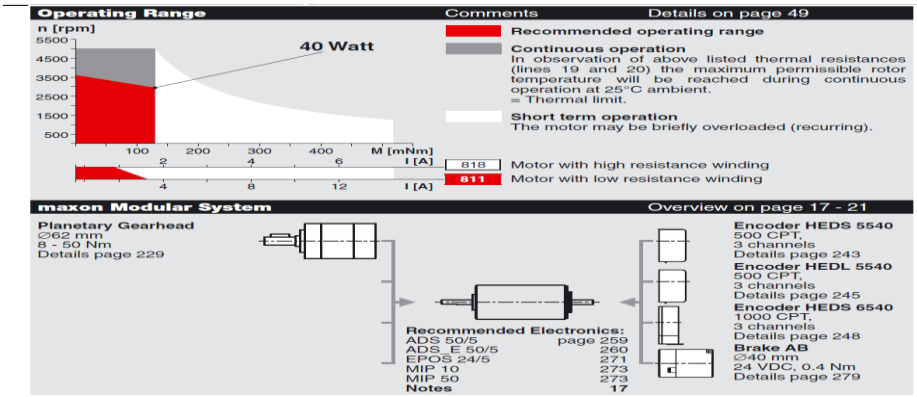

Figure 6: Range of Operation

Table 2: Motor Specifications

Specifications		
Axial play at axial load	< 15 N	≤ 0.1 mm
	> 15 N	0.1 - 0.15 mm
Axial play for motor combinations with encoder is limited to max.		0.15 mm
Preloaded ball bearings		
Preload strength min.		15 N
Max. ball bearing loads		
axial (dynamic)		15 N
radial (5 mm from flange)		100 N
Force for press fits (static)		400 N
(static, shaft supported)		10 000 N
Radial play ball bearing		0.05 mm
Ambient temperature range		-20 ... +100°C
Max. rotor temperature		+125°C
Number of commutator segments		26
Weight of motor		790 g
2 pole permanent magnet		
Values listed in the table are nominal. For applicable tolerances see page 43. For additional details please use the maxon selection program on the enclosed CD-ROM.		

The load torque (friction) is proportional to the speed. It can be expressed as $C_r = K_1\Omega$. K_1 = 0.0005 N*m/(rad/sec). Figure 7 shows the circuit which was simulated using PSIM:

Simulating the circuit above and varying the value of the input voltage V (element in the shaded box) in order to obtain a speed of 1500 rpm in the steady state. The result is 14.5 Volts. Then, recording below the response time at 5 % (T_r) of the final value as well as the armature current (I_a) in the steady state:

T_r = 83 ms I_a = 1.08 A

II. Modeling of the Motor/Load

1. Equations of the motor

The modeling of the unit motor + load is made possible by using the basic equations of the DC machine and the fundamental principle of dynamics. A permanent magnet machine is proposed [13] (with constant flux, no magnetic saturation). Figure 8 shows the equivalent circuit of the system's armature.

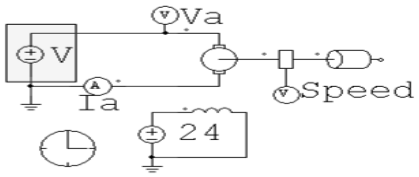

Figure 7: The Simulated Circuit

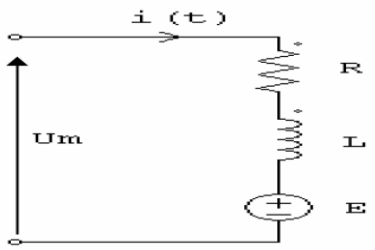

Figure 8: Equivalent Circuit of the System's Armature

The following electrical equations can be deduced in any particular state:

$$U_m(t) = Ri(t) + L\frac{di(t)}{dt} + E(t) \quad (1)$$

(k is *emf* constant which is considered as equal to the torque constant). Here is a reminder of the electromagnetic equations linked to the motor:

$$E(t) = k\Omega(t) \;\; et \;\; C_m(t) = ki(t) \quad (2)$$

Therefore,

$$U_m(t) = Ri(t) + L\frac{di(t)}{dt} + k\Omega(t) \quad (3)$$

Mechanical equations:

Cm: the electromagnetic torque produced by the motor.

J: is the moment of inertia.

f: coefficient of viscous friction.

The fundamental principle of dynamics allows us to write:

$$\frac{d\Omega(t)}{dt} = C_m(t) - C_{ch}(t) \quad (4)$$

Cch: torque load. It consists in the load torque Cr and the friction Cf.

With Cf = fΩ (Dry friction is ignored).

By stating that Cch = Cr + Cf, the equation (4) can be written this way:

$$C_m(t) = J\frac{d\Omega(t)}{dt} + f\Omega + C_r(t) \quad (5)$$

2. Block diagram

The variations in the armature current and the speed (the quantities studied are considered to be nil at the initial instant).

In LAPLACE variables the equations, (4) and (5) become:

Um(s) = (R+Ls)I(s)+kΩ(s) et Cm(s) = (f+ Js)Ω(s) + Cr(s) (6)

Therefore,

$$I(S) = \frac{U_m(S) - k\Omega(s)}{Ls+R} \quad and \quad \Omega(s) = \frac{kI(s) - C_r(s)}{Js+f} \quad (7)$$

The obtained block diagram is shown in Figure 9:

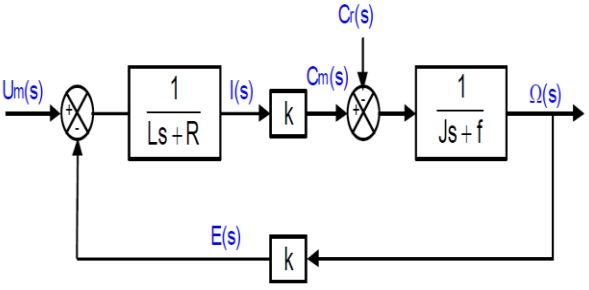

Figure 9: The Obtained Block Diagram

III. Transfer Functions

Control of the speed by the armature, calculation yields:

$$\Omega(s) = k\frac{U_m(s)}{(Js+f)(Ls+R)+k^2} - C_r(s)\frac{(Ls+R)}{(Js+f)(Ls+R)+k^2} \quad (8)$$

In the case of speed control, we consider the load torque as a disturbance and the transfer function in voltage is written:

$$T_\Omega(s) = \frac{\Omega(s)}{U_m(s)} = \frac{k}{(Js+f)(Ls+R)+k^2} \quad (9)$$

A second order transfer function is obtained, where

$$\tau_e = \frac{L}{R} \; and \; \tau_m = \frac{J}{f} \quad (10)$$

The electromechanical time constant is:

$$\tau_{em} = \frac{Rf}{k^2+Rf}\tau m \quad (11)$$

and the coefficient Km

$$K_m = \frac{k}{k^2+Rf} \quad (12)$$

The relation (12) in the domain of common frequencies is:

$$T_\Omega(s) = \frac{1}{K_m}.\frac{1}{(1+\tau eS)(1+\tau emS)} \quad (13)$$

When τe is very small in relation to τem, or several frequencies being predicted are very weak, equation (13) can be concluded to:

$$T_\Omega(s) = \frac{1}{K_m}.\frac{1}{(1+\tau emS)} \quad (14)$$

In this case, the machine is observed as a simple first order (however, it must not be subject to stress too quickly, therefore, a variation in the load causes a modification in the model of the system. Moreover, if the load is large the simplification hypotheses used can turn out to be unsound. Current control by the armature: The block diagram of the previous section can be represented in figure 10:

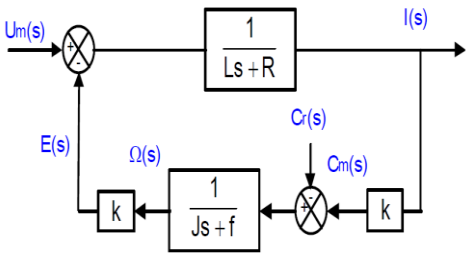

Figure 10: Control Loop of the Armature

This block diagram will be used to study current control (or torque control). It will also be useful to set the parameters of the current circuit in the case of speed control with a secondary loop. If the torque load is a disturbance, the transfer function in current is written:

$$T_I(s) = \frac{I(s)}{U_m(s)} = \frac{Js+f}{(Js+f)(Ls+R)+k^2} \quad (15)$$

This relation can be approached by:

$$T_I(s) = A.\frac{(1+\tau ms)}{(1+\tau es)(1+\tau ems)} \; and \; A = \frac{f}{Rf+k^2} \quad (16)$$

Generally, τm>τem>τe and can be seen that in a closed loop the transfer function is equivalent to that of a first order. In the PSIM circuit as shown in the figure 11 the parameters for the blocks TF1 and TF2 are used. The dc motor parameters in the PSIM schematic in the previous page will be used to derive the parameters for TF1 and TF2. The value of the friction coefficient for Block TF2 is: kf = 5.17 µN*m/(rad/sec).

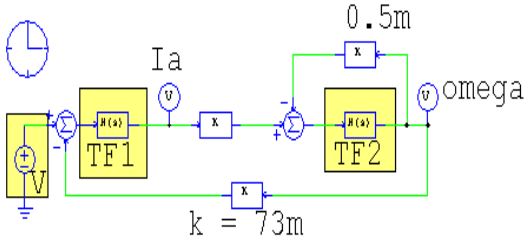

Figure 11: The PSIM Circuit

For the TF1 block:

B_1 =0 A_1 =0.92m

B_0 =1 A_0 =2.85

For the TF2 block:

B_1 =0 A_1 =63.5u

B_0 =1 A_0 =5.17u

Using the input voltage V obtained in the previous page, simulate the circuit and compare the values with those of the previous circuit.

T_r = 80 ms

I_a =1.08 A

By comparing the values of Tr and Ia with values that are obtained in the precedent page, it can be found that in steady state the same results are found than for the first simulation. In the transient analysis the same maximum values during the startup (5A) can be found. Also, For the response time can be seen a small difference between the two simulations (3ms). This difference is caused by either the results precision of the software or because the motor is not a permanent magnet motor. In order to connect the chopper to the motor and load, the technical specifications[13] require a torque ripple of less than 5% (± 2.5% around the nominal operating point). In this section, a check if it is necessary to use a smoothing inductor and what should be the duty cycle of the chopper (α) in order to deliver an average output voltage V equal to the value

calculated earlier (the voltage E is equal to 24 V) is required. It was found that **α** = 14.48/24=0.604. The value of the voltage V_{com} in order to set the duty cycle at the same value as it was found earlier is V_{com} = 0.604*10=6.04V, as shown in figure 12 below:

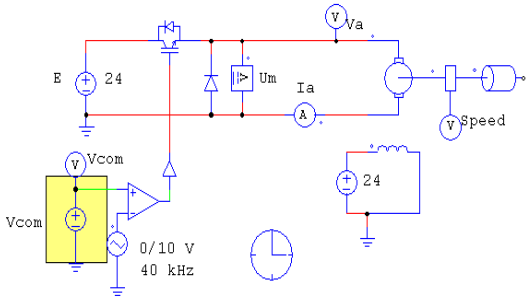

Figure 12: The Modified Circuit

Simulating the circuit with the voltage V_{com} calculated above, and measure U_m (U_m is equivalent to the voltage V calculated previously), the average value of the voltage at the terminals of the motor in the steady state was found to be U_m = 14.4 V and observing the amplitude of the armature current I_a in the steady state. Zooming in and record the minimum and maximum values of the current. The average function in SIMVIEW is employed to obtain the average current ($I_{a\text{-}avg}$)

I_{amax} =1.148 A, I_{amin} =1.002 A, I_{a_avg} =1.07 A. Calculating the torque ripple:

Δ_{Ce} = (1.148-1.002)/1.07=13.6%

It is important to mention that comparing the value of the torque ripple calculated to the technical specifications, it can be concluded that the technical specification is not achieved and the torque ripple is above 5%. Calculating the smoothing inductance required to comply with the technical specifications (the worst-case scenario is at α = 0.5), it was found to be:

dimax=(E*Th)/(4*L)(E=24 ; Th=1/40kHz),

dimax=5%*(Imoy)=0.05*1.08, Thus L=2.8mH as in figure 13

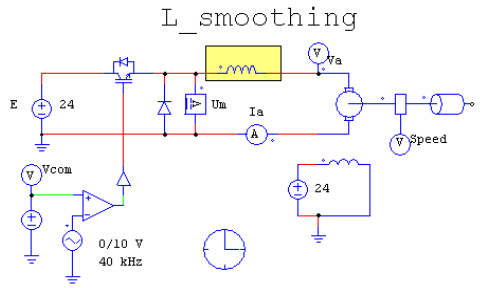

Figure 13: Circuit with Smoothing

In Figure 13, the value of the smoothing inductance is entered and the simulation is run and the results were observed. For the same average value of Ia_avg=1,08 A, DImax was measured 35 mA then DImax/Ia_avg = 3,2 % which is smaller than 5 %. The technical specifications are now satisfied.

III. Control Loop Design

1. Designing the current loop

The theoretical analysis gives the expression of the transfer function of the current in the open loop circuit:

$$T_I(s) = A.\frac{(1+\tau_m s)}{(1+\tau_e s)(1+\tau_{em} s)} \qquad (17)$$

Where τm, τe, and τem are the mechanical, electrical and electromagnetic time constants, respectively. The asymptotic Bode plot of this transfer function is in figure 14 (with $\omega 1 = \frac{1}{\tau_m}$ and $\omega 2 = \frac{1}{\sqrt{\tau_e \tau_{em}}}$).

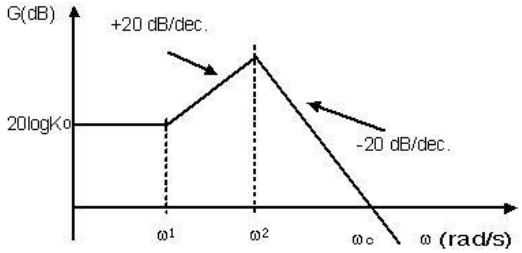

Figure 14: The Asymptotic Plot

The transfer function of the chopper is approximated by a gain G_0 where G_0 = 2.4 (i.e. 24/10). Therefore, K_0 = A x G_0. In Figure 14, a sinusoidal voltage source Vswp is superimposed on top of the operating point. By varying the frequency of the source Vswp, the frequency analysis is performed to obtain the Bode plot. The values of the mechanical and electrical time constants can be calculated in order to determine the frequency range of the AC sweep, the results are found to be f_m = 13mHz and f_e = 122.4 Hz,

Since $\tau_m = \frac{J}{f}$, then with J = 63,5 10^{-6} kg.m^2 and f = 5,17 mNm/rad.s^{-1} , t_m = 12,3 s then

$$f_m = \frac{1}{2\pi \times 12{,}3} = 13\,\text{mHz}$$ and

$$\tau_e = \frac{L_{tot}}{R}$$

With L_{tot} = 0,92 10^{-3} + 2,8 10^{-3} = 3,72 mA and R = 2,85 W, then t_e = 1,3 ms and

$$f_e = \frac{1}{2\pi \times 1{,}3\,10^{-3}} = 122{,}4\,\text{Hz}$$

The start frequency is set and the end Frequency of the AC sweep in the circuit in figure 15 (respectively to 1Hz and to 1kHz), and running the simulation.

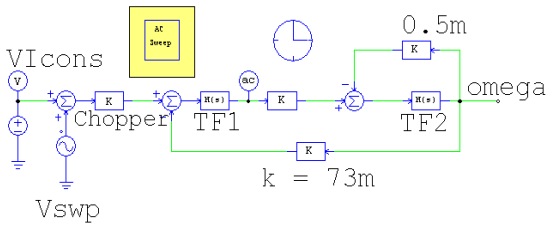

Figure 15: The Simulation with AC Sweep

The diagram of the circuit gain is coherent with the asymptotic diagram. It can check that for high frequencies the attenuation is -20 dB per decade. Therefore, it can assert that in a closed loop and consider the transfer function a first order system function. A PI type controller is selected with an integration time constant T_i so that $T_i = 1/\omega_2$ as in the asymptotic plot in figure 14. Moreover, a response time, t_r is set, at 95 % in a closed loop so that t_r = 1 ms bearing in mind that for a first order system as follows:

$$t_s = \frac{3}{\omega_0} \qquad (\omega_0 = \text{cut-off frequency})$$

On the Bode diagram obtained earlier, locate the frequency ω_2 and calculate Ti.
w_2 = 628.3 rad/sec, $T_i = 1/\omega_2$ = 1.6 ms

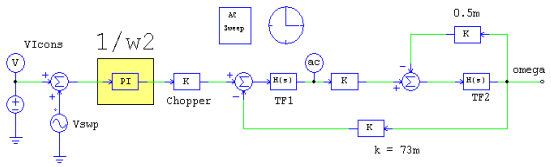

Figure 16: The Circuit with PI Controller

In the Figure 16, parameters for the PI controller as: $T_i = 1/\omega_2$ and K_p=1. Simulating the open loop circuit and calculating the value of ω_0 in order to obtain a response time equals to 1 ms.
ω_0 = 3000 rad/sec
Therefore
f_0 = 477.5
Measuring the value of the circuit gain at the frequency f_0.

$G_{f(0)}$ = -13.44 dB
Determining the value of K_p which will achieve a gain of 0 dB at the frequency f_0.
K_p = 4.7
Thus, to have at f_o a gain equals to zero, it needs an additional amplification of 13,44dB =20log(K_p)
Then, K_p=10e(13.44/20)=4.7
The calculations can be confirmed by setting the parameters of the controller again, running the simulation, and observing the step response in a closed loop in the time domain.

2. Design of the speed loop:

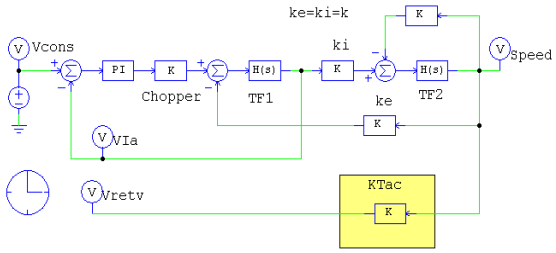

Figure 17: Circuit with Speed Loop

In Figure 17, Calculating the scaling factor Ktac, so that for V_{cons} = 5 V, a speed equals to 1500 rpm.
K_{tac} = 31.83mV/rad.s(-1) Where, Ktac= 5/(1500*2*PI/60)
Running the simulation and observing the signal V_{cons} (speed reference) and V_{retv} (speed feedback). Then by using the resource document identify the time constant τ, as well as the circuit gain for the loop K (in the steady state).
τ = 128 ms, K= 4.6
Determining the parameters, A and T_i of the PI type controller (series) that ensures a response time T_r in a closed loop of approximately 100 ms.
K_B = 6.68, A = 1.45, T_i = 58ms, Because: Tr= 6*t/(1+Kb)

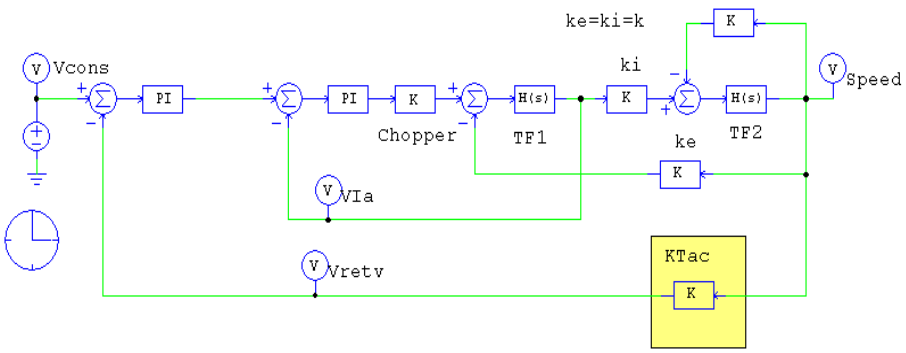

Figure 18: The Circuit with the Ktac Parameter

In Figure 18, the parameter Ktac is used, and the closed loop circuit is simulated. It was found that the system is stable.

3. Results

For the previous circuit diagram (closed loop with controller), the simulation is applied again to visualize the amplitude of the current in the motor. The maximum value of the current in transient state was found to be I_{amax} = 6.7A.

Simulating the circuit in Figure 19 with the limiter in the open loop transfer function that limit the current amplitude at 3 A. Then run the simulation again and observe the effect of this limitation.

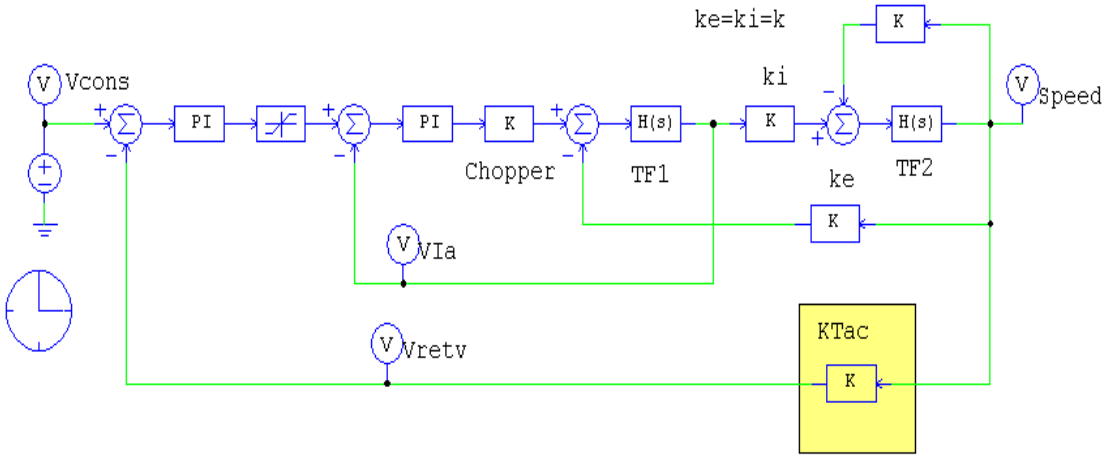

Figure 19: Limiter is set to 3A

With the models of different parts of the system, the relationship between different variables and design the control loops can be studied. The study is concluded (before implementation) by simulating the complete system, as shown in Figure 20.

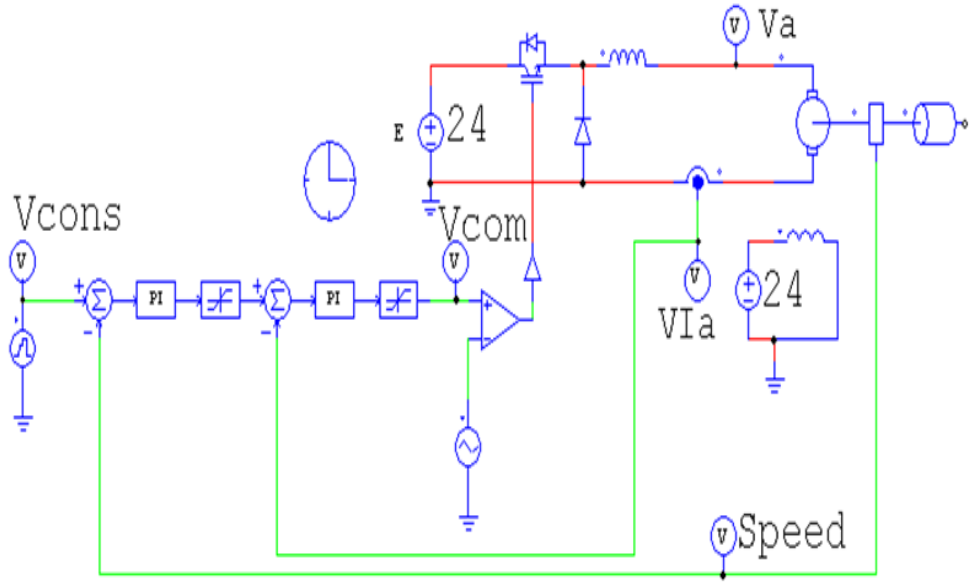

Figure 20: Simulation of the Complete System

Carrying out a test with the change of the speed reference up to 3000 rpm (V_{cons} = 10 V). In these conditions, the motor is operated at its nominal power. At last, the simulation is run and observed the speed reference, the actual speed, and the armature current. The results showed that for Vcons=10V, the motor does not reach the requested speed, and in order to fix this problem the power voltage must be increased from 24V to 30V. This study may be continued in many ways such as from the modelling point of view, we could take into account the response time of the chopper, the necessary filtering of disturbances affecting the tachogenerator, the hysteresis affecting the comparator or a possible galvanic insulation between the power and the command sections or even operating in the four quadrants. However, for complex structures and for wide frequency ranges, it is much faster with the transfer function block diagram.

4. Conclusion

The use of chopper circuit as converting device is convenient for the control of the motor's speed and PI model, speed and current controller by using simple closed loop system for the beginning. This is a remarkable controller based on the results. The main approach is to study the rated current and speed controller and then a common model of the individually excited dc motor is created so that we obtain a universal DC drive system and a design for current and speed controller. Moreover, the simulation outcome showed that the assumed controller provides higher performance and less settling time under varying reference speed or load, which is quite essential for aircraft maneuvering purposes. In future research, the overshoot issue can be eliminated if a PID controller or Fuzzy approach is utilized. With the models of different parts of the system, the relationship between different variables, and design the control loops can be studied.

Nomenclature

Ω	Rotational Speed
C_r	Load Torque
K_1	Friction Constant
Cm	electromagnetic torque
J	Moment of Inertia
Cch	torque load
f	coefficient of viscous friction
UAV	Unmanned Aerial Vehicle
Ktac	Scaling factor

References

[1] B.K. Bose, "Power Electronics and Motor Drives–Recent Technology Advances," Proceedings of IEEE International Symposium on Industrial Electronics ISIE, pp. 22-25, 2002.

[2] G.K. Dubey, "Fundamentals of electrical drives," CRC Press, 2002.

[3] Z. Zhu, D. Howe, C. Chan, "IEEE Transactions on Magnetics," pp. 229-238, 2002.

[4] R. Krishnan, "Electric motor drives: modeling, analysis, and control," Prentice Hall, 2001.

[5] W. Hong, W. Lee, B.-K. Lee, "Dynamic simulation of brushless DC motor drives considering phase commutation for automotive applications," 2007 IEEE International Electric Machines & Drives Conference, IEEE, pp. 1377-1383, 2007.

[6] K. Yeung, J. Huang, "Computers in Industry," pp. 305-311, 2003.

[7] J.H. Boyd, G. Duncan, M.T.G. Perry, "Brushless DC motor control," Google Patents, 2000.

[8] M. Pahlevaninezhad, P. Das, G. Moschopoulos, P. Jain, "Sensorless control of a boost PFC AC/DC converter with a very fast transient response," Applied Power Electronics Conference and Exposition (APEC), 2013 Twenty-Eighth Annual IEEE, IEEE, pp. 356-360, 2013.

[9] Y. Cho, K.-B. Lee, M. Li, J.-H. Song, Y. Lee, "Novel torque predictive control for a permanent-magnet synchronous motor with minimum torque ripple and fast dynamics," Applied Power Electronics Conference and Exposition (APEC), 2013 Twenty-Eighth Annual IEEE, IEEE, pp. 2253-2258, 2013.

[10] N.N. Lima, L.C. de Freitas, G.M. Buiatti, J.B. Vieira, L.C. Freitas, E.A. Coelho, "Low complexity system for real-time determination of current-voltage characteristic of PV modules and strings," Applied Power Electronics Conference and Exposition (APEC), 2013 Twenty-Eighth Annual IEEE, IEEE, pp. 2817-2823, 2013.

[11] M. Hilmy, M. Orabi, M.E. Ahmed, M. El-Nemr, M. Youssef, "A less sensor control method for standalone small wind energy using permanent magnet synchronous generator," Applied Power Electronics Conference and Exposition (APEC), 2011 Twenty-Sixth Annual IEEE, IEEE, pp. 1968-1974, 2011.

[12] M. Owayjan, R.A.Z. Daou, X. Moreau, "A novel approach to compare a Sliding Mode Controller with a CRONE Controller in frequency domain: Application to a linear DC motor," Multidisciplinary Conference on Engineering Technology (IMCET), IEEE International, IEEE, pp. 196-201, 2016.

[13] A.L. Bencsik, J.F. Bito, L. Horvath, I.J. Rudas, "Mathematical model based investigation on DC servo robot drives, Industrial Electronics, Control, and Instrumentation," 1995., Proceedings of the 1995 IEEE IECON 21st International Conference on, IEEE, pp. 81-86, 1995.

[14] Z. Zhu, D. Howe, "IEEE Transactions on energy conversion," pp. 407-412, 2010.